Thermodynamic and Kinetic Investigations for Redox Reactions of Nickel Species Supported on Silica

Shohei Yamashita, Misaki Katayama, Yasuhiro Inada

Graduate School of Life Sciences, Ritsumeikan University, 1-1-1 Noji-Higashi, Kusatsu, 525-8577, Japan

Abstract

The redox mechanisms of Ni catalysts supported on various SiO_2 have been studied to evaluate the effects from the structure of supporting materials. The mesoporous silica (MCM-41 and SBA-15) was used as the supporting material in addition to the other silica with different surface area. The Ni loading (5, 10, and 15 wt%) was varied to clarify the effect from the Ni particle size. The structure of Ni species on SiO_2 was analyzed by *in-situ* XAFS experiments under oxygen or hydrogen atmosphere at elevated temperature. The dynamic processes were captured by the time-resolved dispersive XAFS (DXAFS) technique under the reaction conditions. The supported NiO species was quantitatively reduced to the metallic Ni(0) species on all silica except for SBA-15. It is found that the reduction of NiO does not fully proceed in small meso pore of SBA-15. The observed reaction kinetics shows that the redox processes are composed of the surface reactions of Ni particles and the successive oxygen migration in the particle between the core and the surface. The first-order kinetics on Ni suggests that the latter process is the rate-determining step for overall redox reactions. The rate constant is dependent on the particle size, which is related to the surface area. The mesoporous structure of the supporting material contributes to the redox rate of Ni species by varying the particle size of the supported Ni species. For the reduction of supported NiO, the observed first-order kinetics is different from that of PdO, for which the observed zero-order kinetics on PdO is explained by the faster oxygen migration in the PdO particle rather than the surface reduction. The mechanical disagreement between PdO and NiO supported on silica is ascribed by the crystal structure difference.

1. Introduction

The supported catalysts play important roles in the modern society. The toxic compounds in gas emissions from industrial factory are converted into nontoxic gases by means of heterogeneous catalysts with supported metal species. All automobiles are equipped with the catalysis converter to reduce the toxic components in the exhaust gas. The chemical industry uses metal catalysts supported on oxides to generate useful materials for the human society. For such purposes, it is well known that the rare metals, such as Pd, Pt, and Rh, show high catalytic activity for many chemical processes. The finding and utilization of alternative catalysts using more widely available elements, such as Ni, Fe, and Mn, is thus very important and urgent subject for recent society because of the lack of rare and expensive metal elements.

The Ni catalysts supported on SiO_2 are used to generate H_2 by the CO_2 or steam reforming reaction of alkane, and the reactions are also important to solve the energy problems of the modern society [1]. The supported Ni catalysts on SiO_2 show good conversion performance for many chemical processes, but the efficiency and the lifetime are largely dependent on the particle size of the active Ni species supported on SiO_2. The speciation of the Ni species in the atomic scale under the reaction conditions is thus necessary to understand the properties of the Ni catalyst, because the chemical reactivity is directly related to the chemical state of the active Ni species.

It is important for supported catalysts to understand the electronic state and the local structure of the active species. The understanding of reaction mechanisms at the atomic scale is useful information to restrain side reactions, to achieve higher activity, and to maintain longer lifetime for a target chemical reaction. The X-ray absorption fine structure (XAFS) is a powerful technique for heterogeneous catalysts. The local structural information for a supported metal element is selectively available from those of a large amount of coexisting supporting materials by the analysis of the extended X-ray absorption fine structure (EXAFS). The feature of X-ray absorption near edge structure (XANES) is sensitive to the electronic state of a supported metal element. In addition, because the XAFS spectroscopy is applicable to *in-situ* measurements, the electronic state and the local structure can be analyzed for a supported metal element under the reaction conditions, which is crucial to understand the chemical property of the supported catalyst. Furthermore, an application of the time-resolved dispersive XAFS (DXAFS) technique with the time resolution of ms is very useful to evaluate the reaction mechanisms by the kinetic analyses.

In this study, the redox mechanisms of the supported Ni species have been investigated by the *in-situ* XAFS and DXAFS experiments using various SiO_2 with different structures. Because the Ni catalysts are exposed under an oxidative or a reductive atmosphere in the catalysis processes, the speciation of Ni species has been carried out under O_2 or H_2 gas atmosphere at elevated temperature as the most basic model condition. The kinetic analyses

for redox reactions have been carried out by the time-resolved DXAFS technique. The information is expected to become the fundamental aspect to resolve the catalysis mechanisms proceeded on the Ni particle under much complex reaction conditions for the actual catalysis systems.

2. Experimental

The supported Ni catalysts were prepared by the impregnation method using 4 types of SiO_2, *i.e.*, SiO_2 distributed by the Catalysis Society of Japan (JRC-SIO-10: **S1**), commercially available SiO_2 (Aldrich, **S2**), prepared mesoporous SiO_2 (MCM-41: **S3** and SBA-15: **S4**). The specific surface area of the supporting SiO_2 was 190 m^2/g for **S1**, 390 m^2/g for **S2**, 900 m^2/g for **S3**, and 720 m^2/g for **S4**. The Ni loading on **S1** was changed to be 5, 10, and 15 wt%, while those on the other SiO_2 were kept to be 10 wt%.

The *in-situ* XAFS measurements were carried out at BL-3 of the SR center (Ritsumeikan University), and BL-9A and -12C stations of Photon Factory (PF, High Energy Accelerator Research Organization) at the Ni K edge in the transmission mode. The Si(111) double-crystal monochromator was detuned to remove higher-order harmonics at PF. The quick-scanning mode was applied for all measurements. Sample powder was first treated in the *in-situ* cell with the diluted H_2 gas flow at 873 K, and was cooled to room temperature by keeping the gas flow. The gas was changed to the diluted O_2 (10 vol% balanced by He, 200 cm^3/min), and the sample was heated to 873 K at 10 K/min (temperature-programmed oxidation: TPO). Thereafter, the sample was cooled to room temperature by keeping the gas flow, and then the gas was changed to the diluted H_2. The sample was heated again to 873 K at 10 K/min (temperature-programmed reduction: TPR). The quick-XAFS measurements were carried out during these processes with the time interval of 2 min.

The DXAFS measurements were carried out at NW2A station of PF-AR (KEK) [2]. Polychromatic X-rays were obtained with a Si(111) bent crystal (Bragg type) and were detected by a linear photodiode array detector equipped with a scintillation (CsI:Tl). Sample powder was placed in an *in-situ* cell for the DXAFS measurements, and the O_2 or H_2 gas was rapidly introduced into the evacuated cell at 873 K to follow the redox processes of Ni species. DXAFS spectra were recorded every 30 ms.

3. Results and discussion

3-1. Thermodynamic analysis of supported Ni species on various SiO_2.

An example of the XANES spectral change is shown in Figure 1 for the TPO and TPR processes on **S1** from room temperature to 873 K. The initial XANES spectrum of the TPR process is perfectly consistent with that of NiO, and is almost in accordance with the final spectrum of the TPO process. Similarly, the XANES spectrum after the TPR process is in

agreement with that of Ni metal, and is in accordance with the final spectrum of the previous TPO process. The similar spectral changes were observed in spite of the Ni loadings on three SiO_2 of **S1**, **S2**, and **S3**. These results suggest that the redox reactions between NiO and Ni metal particles proceed qualitatively and reversibly at 873 K. In contrast, the NiO reduction on **S4** does not proceed quantitatively and the NiO species is partially remained after the treatment under the H_2 flow at 873 K. The smaller pore size of **S4** than **S3** may contribute to resist against the reduction of supporting NiO. It is considered that the diffusion of H_2 molecules into the deep area of small pore is energetically difficult, and thus the reduction of NiO particles involved in the small pore of **S4** proceeds imperfectly, resulting to the mixture of metallic Ni(0) and NiO particles after the TPR process.

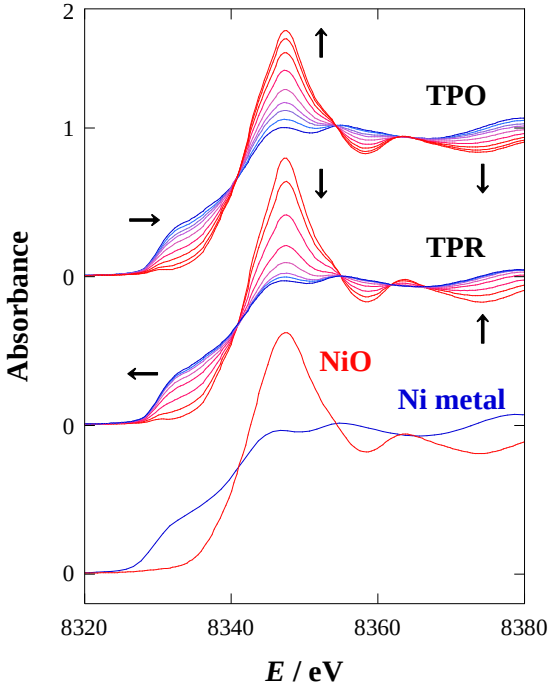

Fig. 1. XANES spectral change during the TPO and TPR processes from room temperature to 873 K on **S1** (15 wt%). The reference spectra of bulk NiO and Ni metal are included.

The structure parameters were determined by the curve-fitting analysis of the EXAFS data. The optimized $N_{Ni–O}$ values are shown in Figure 2 as a function of temperature during the TPO and TPR processes. The oxidation of Ni(0) particles proceeds at around 400 ˚C, but the temperature is slightly varied in response to the Ni loading (Fig. 2A) and the type of SiO_2 (Fig. 2B). The larger loading and the smaller surface area of SiO_2 lead to higher oxidation temperature, suggesting that the larger Ni(0) particle needs higher temperature to be oxidized. It is found that such temperature difference is not obvious for the reduction process, indicating the similar particle size of NiO. Almost same values of $N_{Ni–O}$ at the beginning of TPR support the comparable NiO particle size.

3-2. Kinetic analysis of supported Ni species on various SiO_2.

An example of the dynamic spectral change is given in Figure 3 for the DXAFS experiments of redox reactions at 873 K. It has been confirmed that the XANES spectrum is perfectly consistent with that of NiO before the injection of H_2 gas, and thus NiO is quantitatively reduced to Ni(0) on **S1**, **S2**, and **S3**. As observed in the TPR and TPO

experiments (*vide supra*), the NiO reduction is not completed on **S4** with small pores.

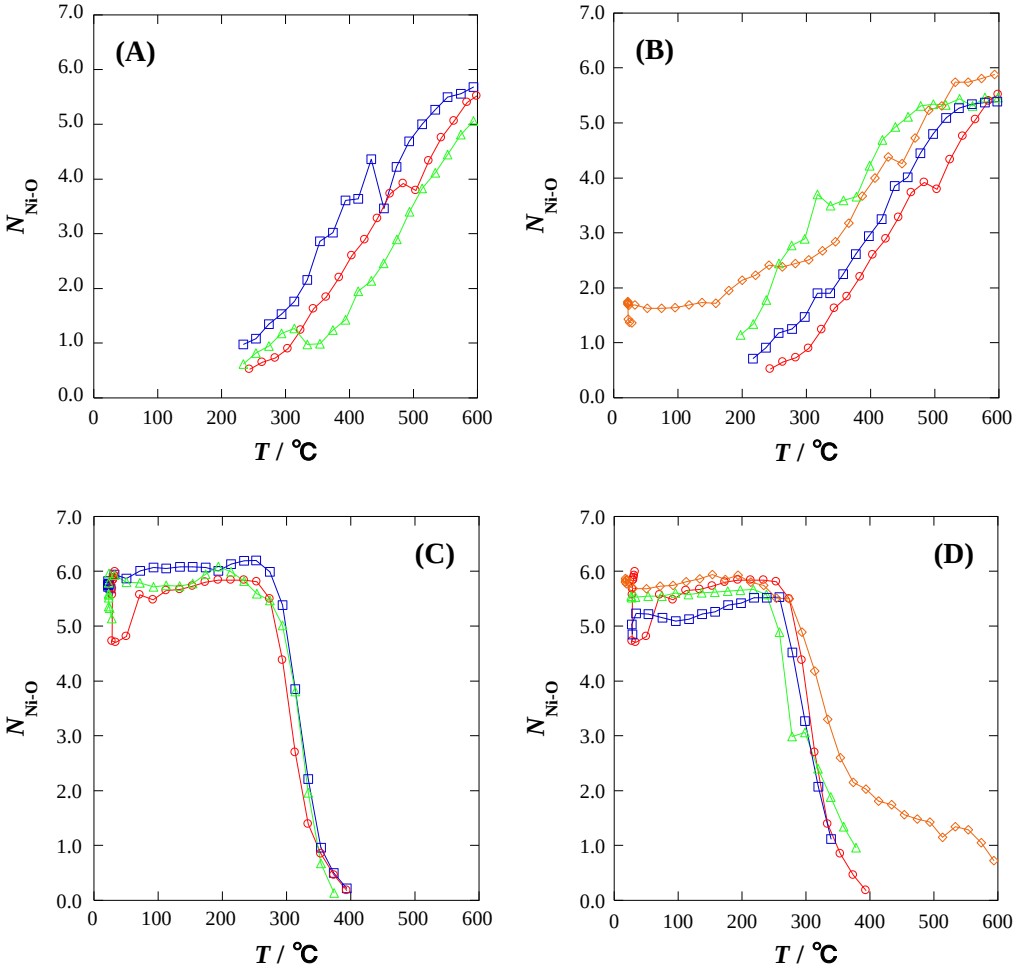

Fig. 2. The coordination number (N_{Ni-O}) of Ni-O determined by the EXAFS analysis is plotted versus temperature for the TPO (A and B) and TPR (C and D) processes. The optimized N_{Ni-O} values on **S1** are depicted for the sample with the Ni loading of 5 wt% (blue squares), 10 wt% (red circles), and 15 wt% (green triangles) in A and C. The corresponding values on **S1** (red circles), **S2** (blue square), **S3** (green triangles), and **S4** (orange diamonds) are shown in B and D.

The X-ray absorbance changes at 8345 eV, which corresponds to the white line peak of NiO, are shown in Figure 4 as a function of time. Two-phase changes are observed for both the oxidation and reduction processes. The first reaction, which is completed within *ca*. 5 s, corresponds to the oxidation/reduction step because of the large spectral change, indicating the valence change on the Ni atoms. The sintering of the formed NiO or Ni(0) particle is considered to proceed at the slow second step in the order of minutes. The absorbance change during the first redox step is well reproduced by a single-exponential function. The conditional first-order rate constants (k_{obs}) were determined by the optimization of the

single-exponential function.

As schematically depicted in Figure 5, the redox process is initiated by the adsorption of reaction gas molecule to the supporting SiO_2. The adsorption equilibrium constant is represented by K_A. In the case of oxidation (Fig. 5A), the surface Ni(0) species (Ni*) is oxidized by an adsorbed O_2 molecule with the rate constant of k_1 to form the surface NiO species (NiO*), which is reversely reduced with the rate constant of k_{-1}. A oxygen radical generated as an intermediate is considered to react quickly with peripheral surface Ni* species. The internal O atom is migrated with the rate constant of k_2 from surface NiO* to Ni(0) core, leading to the regeneration of Ni*. The change of the number of NiO* (N_{NiO*}) is given by Equation (1),

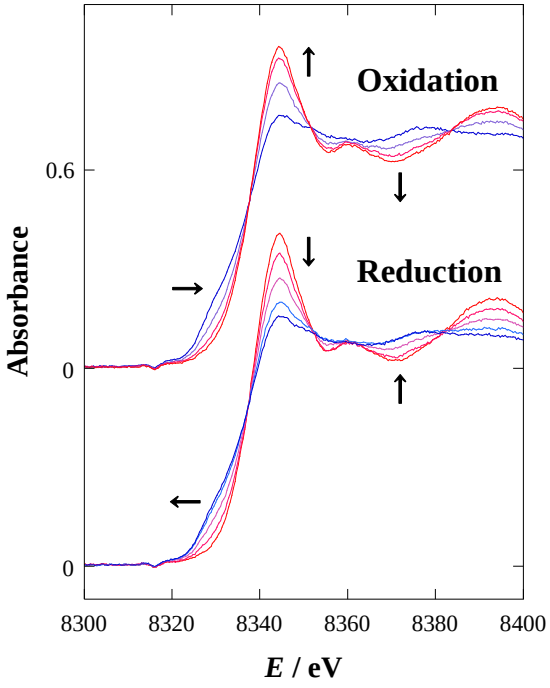

Fig. 3. Dynamic XANES change during oxidation (upper) and reduction (lower) process at 873 K after the rapid injection of O_2 and H_2 gas (9.3 kPa) for the Ni catalyst (5 wt%) supported on **S1**, respectively.

$$\frac{dN_{NiO^*}}{dt} = k_1\theta_{O_2}N_{Ni^*} - k_{-1}N_{NiO^*} - k_2N_{NiO^*}N_{Ni} \quad (1)$$

where θ_{O2} is the surface coverage of O_2 and N_X denotes the number of species X. Assuming the steady state to the NiO* species, the N_{NiO*} term is represented by Equation (2) if the k_2 step is much slower than k_1 and k_{-1},

$$N_{NiO^*} = \frac{K_1\theta_{O_2}N^S}{1+K_1\theta_{O_2}} \quad (2)$$

where K_1 represents the equilibrium constant of the surface reaction ($K_1 = k_1/k_{-1}$) and N^S is the total number of surface nickel species ($N^S = N_{NiO*} + N_{Ni*}$). The conditional first-order rate constant (k_{obs}) is derived as Equation (3) by assuming constant N^S versus time.

$$-\frac{dN_{Ni}}{dt} = \frac{k_2K_1\theta_{O_2}N^S}{1+K_1\theta_{O_2}}N_{Ni} = k_{obs}N_{Ni} \quad (3)$$

The oxygen pressure dependence of k_{obs} is thus expected to show a saturating behavior as a function of O_2 pressure (P_{O2}). The k_{obs} values were plotted versus P_{O2} in Figure 6, in which the saturating dependence is clearly demonstrated. The limiting value of k_{obs} under high O_2 pressure is then approximated to Equation (4),

$$k_{obs} \approx k_2K_1N^S \quad (4)$$

where the $K_1\theta_{O2}$ term is treated to be much smaller than 1, because clear isosbestic points were observed during the oxidation reaction (see Fig. 3). The overall oxidation process of a Ni(0) particle is decomposed into two successive steps, *i.e.*, surface oxidation and oxygen migration, and the kinetic derivation is successfully reproduced the first-order change on Ni and the saturating dependence of k_{obs} versus P_{O2} by assuming the rate-determining oxygen migration.

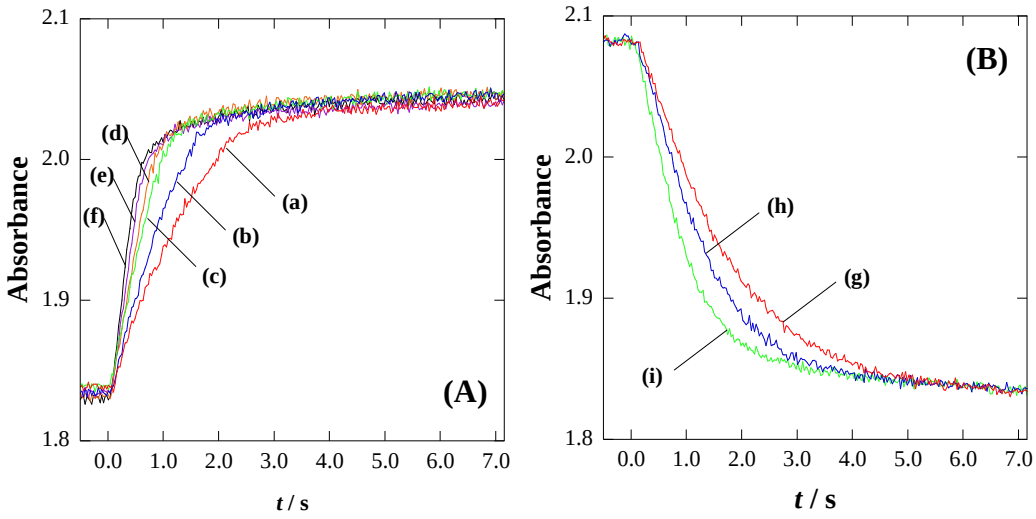

Fig. 4. The X-ray absorbance at 8345 eV is plotted versus time during the oxidation (A) and reduction (B) process at 873 K on **S1** (5 wt%). In A, the O_2 pressure was 1.7 kPa (a), 2.7 kPa (b), 4.2 kPa (c), 6.3 kPa (d), 9.4 kPa (e), and 14.0 kPa (f). In B, the H_2 pressure was 2.6 kPa (g), 4.1 kPa (h), and 9.4 kPa (i).

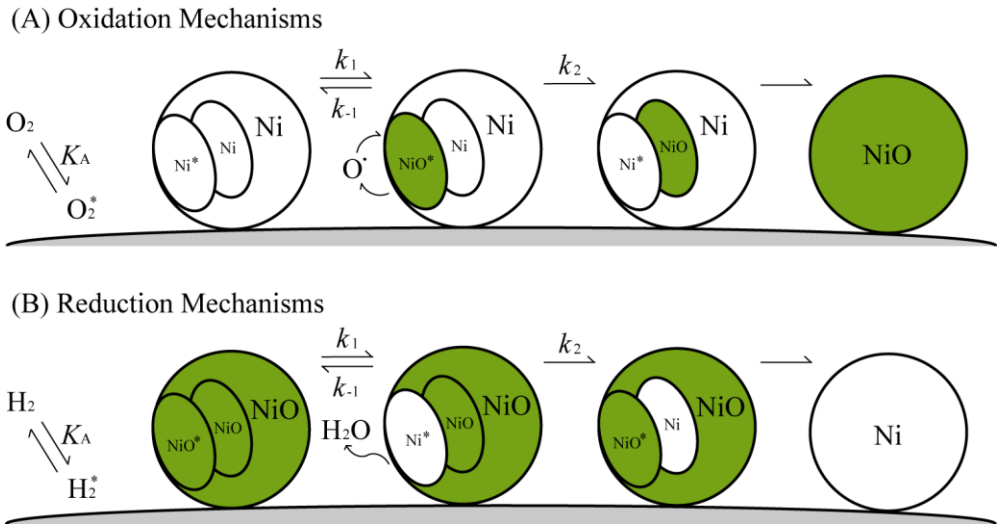

Fig. 5. The concept of redox mechanism of supported Ni species on SiO_2 for oxidation by O_2 (A) and reduction by H_2 (B). The surface component of the particle is labeled with *.

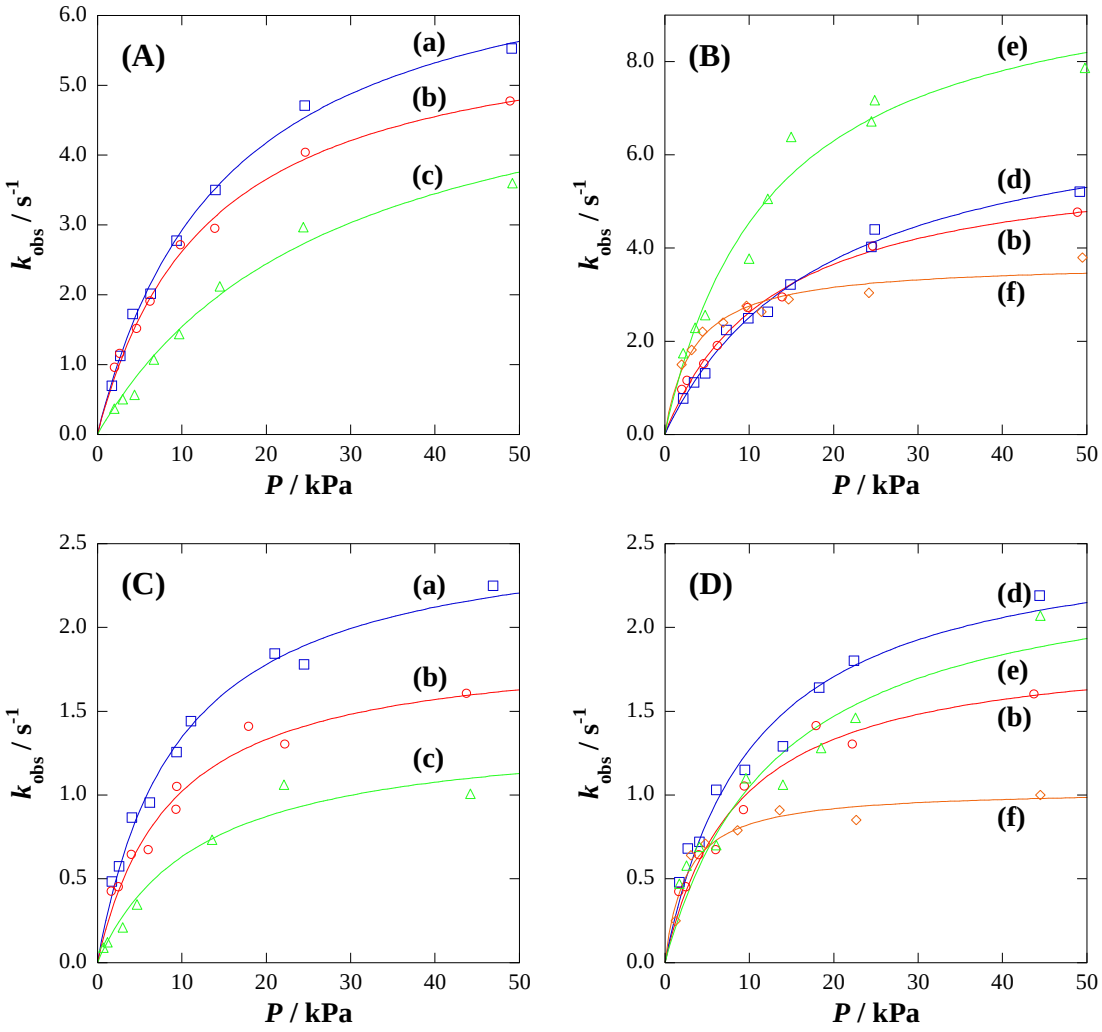

Fig. 6. The conditional first-order rate constants (k_{obs}) as a function of the gas pressure are plotted for the oxidation process (A and B) and reduction process (C and D). The k_{obs} values on **S1** are represented for the Ni loading of 5 wt% (a, blue squares), 10 wt% (b, red circles), and 15 wt% (c, green triangles) in A and C. In B and D, the determined values are given for **S1** (b), **S2** (d), **S3** (e), and **S4** (f).

The reduction of NiO is similarly described in terms of the two successive steps. As show in Figure 5B, the surface NiO species (NiO*) is reduced by an adsorbed H_2, and the oxygen atoms in the NiO particle are migrated with the rate constant of k_2 from the NiO core to the surface, leading to the regeneration of NiO*. It is reasonable to consider that the formed H_2O molecule is evaporated and removed at 873 K. As a result, the H_2 pressure dependence of k_{obs} is expected to show a saturating behavior as expressed by the derived Equation (5).

$$-\frac{dN_{NiO}}{dt} = \frac{k_2 K_1 \theta_{H_2} N^S}{1+K_1\theta_{H_2}} N_{NiO} = k_{obs} N_{NiO} \quad (5)$$

The limiting value of k_{obs} under high H_2 pressure is also approximated to Equation (4),

because some isosbestic points are clearly observed during the reduction of NiO (see Fig. 3), *i.e.*, the $K_1\theta_{H2}$ term is negligible. The saturating dependence has been clearly demonstrated in Figure 6C and D.

The present kinetic investigations first clarify that the limiting k_{obs} value for the Ni catalyst with low Ni loading is larger than that with high Ni loading, indicating that the migration of internal O atom is relatively fast for small Ni particles. This may be related to the migration distance. In addition, it is found that the limiting k_{obs} values on **S3** and **S4** with porous structure are relatively smaller than those on **S2**, although the surface area of **S3** and **S4** is larger than **S2**, implying that smaller particles are expected on **S3** and **S4**. Equation (4) describes that the limiting k_{obs} value is represented by the product of K_1 and k_2. The porous structure of SiO_2 may reduce the K_1 value because of the unfavorable gas diffusion into the pore, resulting to the decrease in the limiting k_{obs} value. The smaller k_{obs} value for **S4** than **S3** is reasonably interpreted by the difference of the pore size. The reaction mechanisms have been clarified for the first time by applying the kinetic analysis to the solid-phase redox reactions for the supported Ni catalysts on various SiO_2.

3-3. Comparison of reduction mechanism between NiO and PdO

The previous investigation for reduction mechanisms of supported PdO on γ-Al_2O_3 [3] shows the combined first- and zero-order rate law on PdO as shown in Figure 7, in which the X-ray absorbance changes are compared between NiO and PdO. The reaction scheme for PdO is the same with that for NiO shown in Fig. 5B, but the zero-order dependence observed for PdO is ascribed by the faster oxygen migration in the PdO particle than the rate-determining surface reduction. The mechanistic difference between NiO and PdO is explained by the structural difference as shown in Figure 8. The O atoms in PdO are arranged in a plane [4], while the O and Ni atoms are alternatively arranged in the rock salt structure of NiO [5]. The planar arrangement of O atoms for PdO is obviously preferable for the O atom migration in the oxide particle. The faster migration for PdO results in the rate-determining surface reduction, which explains the zero-order kinetics for the reduction reaction of supported PdO.

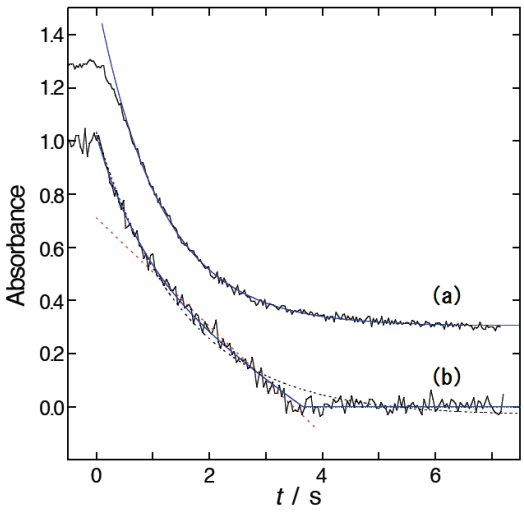

Fig. 7. The X-ray absorbance change for NiO (a) and PdO (b) plotted as a function of time during reduction process.

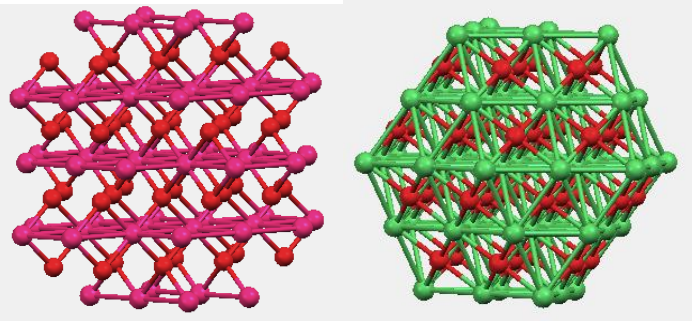

Fig. 8. The crystal structure of PdO (left) and NiO (right). The Pd, Ni, and O atom is depicted by the pink, green, and red sphere, respectively.

4. Conclusion

In this study, the redox mechanisms of the Ni species supported on various SiO_2 has been studied in the atomic scale by means of XAFS techniques. The structure change of the Ni species has been clarified by *in-situ* XAFS experiments, and the dynamic processes have been captured by the time-resolved DXAFS technique under the reaction conditions.

The quantitative and reversible conversion between NiO and Ni(0) has been observed on all silica used in this study, while the reduction of NiO on **S4** does not proceed quantitatively, because the small pores of **S4** inhibit the surface diffusion of H_2 gas. The particle size of Ni(0) is affected by the Ni loading and the surface area of the supporting silica. The higher loading and the smaller area lead to the larger Ni(0) particle, and then the oxidation to NiO proceeds at higher temperature.

The kinetic analyses reveal the reaction mechanisms for the solid-phase redox reactions between NiO and Ni(0). The reactions are composed of the surface oxidation/reduction and the successive oxygen migration in the Ni particle. The first-order kinetics on the Ni species suggests that the latter process is the rate-determining step. The kinetic results indicate that the rate constant is dependent on the particle size of the Ni species, which is related to the Ni loading and the surface area of SiO_2. The mesoporous structure of **S3** and **S4** also contributes to the reduction of rate constants. The clear mechanistic difference has been observed for the reduction of NiO and PdO. The layered structure of PdO may contribute to the fast migration of O atoms in the PdO particle.

Acknowledgment

A part of this work was carried out under the approval of the Photon Factory Program Advisory Committee (Proposal No. 2011G531) of High Energy Accelerator Research Organization.

Reference

[1] J. Sun, X. Qiu, F. Wu, W. Zhu, W. Wang, and S. Hao, *Int. J. Hydrogen Energy*, **29**, 1075 (2004).

[2] Y. Inada, A. Suzuki, Y. Niwa, and M. Nomura, *AIP Conf. Proc*., **879**, 1230 (2006).

[3] M. Katayama, Y, Niwa, K. Doi, S. Yamashita and Y. Inada, *J. Phys. Conf. Ser*., in press.

[4] J. T. Hirvi, T.-J. J. Kinnunen, M. Suvanto, T. A. Pakkanen, and J. K. Nørskov, *J. Chem. Phys*., **133**, 084704 (2010).

[5] J. M. McKay and V. E. Henrich, *Phys. Rev. B: Cond. Matter Mater. Phys*., **32**, 6764 (1985).